

### Structural defects and charge carrier mobility in homoepitaxial layers grown on (100) plane of $\beta$ -Ga<sub>2</sub>O<sub>3</sub>

PIs Martin Albrecht (C1.4), Günter Wagner (C3.5), Klaus Irmscher (C4.4), Zbigniew Galazka (C3.1)

**Research team** Robert Schewski, Michele Baldini, Andreas Fiedler

In the last years  $\beta$ -Ga<sub>2</sub>O<sub>3</sub> has gained intensive interest in the research community, especially as a new material for high power electronic devices. Two different figures of merit show how well suited a material is for power electronics: The Baliga figure of merit (BFOM) estimating dc conduction losses and Huang's material figure of merit (HMFOM) incorporating dynamic switching losses. Both have in common to include the break down field ( $E_c$ ) as a function of  $E_c$ . [3] With a band gap of 4.9 eV resulting in a theoretical  $E_c$  of 8 MV/cm and the possibility to achieve a high conductivity by n-type doping,  $\beta$ -Ga<sub>2</sub>O<sub>3</sub> has a BFOM which is a factor of 3 larger than GaN, a factor of 10 larger than 4H-SiC and factor of 3400 larger than Si. HMFOM is same order as GaN. In contrast to other wide band gap semiconductors in the field (e.g. SiC and GaN),  $\beta$ -Ga<sub>2</sub>O<sub>3</sub> has the advantage that bulk single crystals with high structural perfection can be grown from the melt[1,2] at relatively low production costs which gives the possibility of scaling the manufacturing process. The availability of native substrates obtained from bulk  $\beta$ -Ga<sub>2</sub>O<sub>3</sub> single crystals, enables homoepitaxial growth leading to improved device performance compared to heteroepitaxial growth. Hence, a better understanding of  $\beta$ -Ga<sub>2</sub>O<sub>3</sub> concerning growth and fundamental properties is a *conditio sine qua non*.

To achieve material suitable for electronic applications, we studied, in close cooperation between the clusters C3 and C4, the growth of  $\beta$ -Ga<sub>2</sub>O<sub>3</sub> bulk crystals and layers. Bulk single crystals were grown by the Czochralski method in the IKZ and serve as substrates for the homoepitaxial growth of  $\beta$ -Ga<sub>2</sub>O<sub>3</sub> layers by metal organic vapor phase epitaxy (MOVPE) in the IKZ and by MBE at the PDI. The resulting layers were structurally and electrically characterized in the groups Electron Microscopy and Physical characterization at the IKZ, respectively. Because of this close cooperation, device grade material was achieved. It was used for prototype device fabrications by the cluster groups C3.8 and C3.9 in cooperation with external partners.

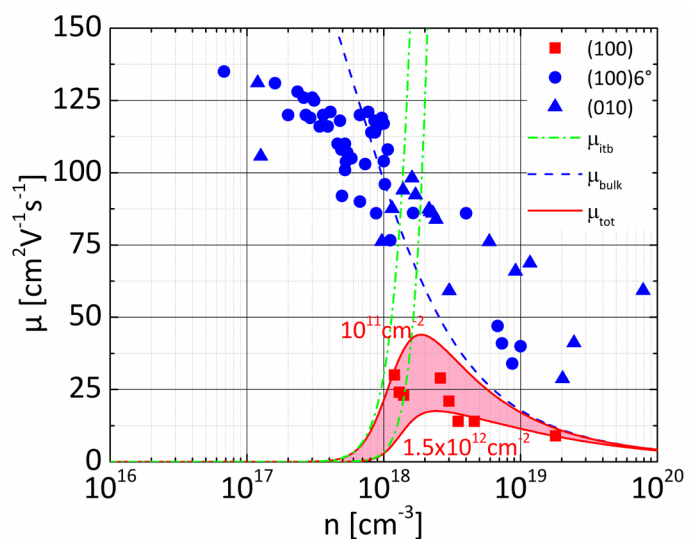


Figure 1 Electron Hall mobility as a function of the electron Hall concentration at 300 K for  $\beta$ -Ga<sub>2</sub>O<sub>3</sub> homoepitaxially grown by MOVPE on (100) oriented substrates (red squares). The blue dashed line represents the calculated bulk mobility after Ma et al.[12] The green dashed-dotted lines represent the calculated mobility due to incoherent twin boundaries of the lowest ( $1 \times 10^{11} \text{ cm}^{-2}$ ) and highest ( $1.5 \times 10^{12} \text{ cm}^{-2}$ ) density determined by TEM. The red-shaded area illustrates the total calculated mobility within these bounds. As blue dots the electron Hall mobility in dependence of Hall concentrations of layers grown on substrates with a miscut angle of  $6^\circ$  are shown. Blue triangles indicate the values for layer grown on substrates with the (010) plane as growth plane.

Si-doped  $\beta$ -Ga<sub>2</sub>O<sub>3</sub> epitaxial layers have been grown on (100)  $\beta$ -Ga<sub>2</sub>O<sub>3</sub> substrates by metal organic vapor-phase epitaxy (MOVPE). Tri-ethyl-gallium (TEGa), molecular oxygen (O<sub>2</sub>) and tetra-ethyl-ortho-silicate were used as Ga, O and Si precursors, respectively. Layers grown at optimized temperature and chamber pressure, i.e. 850° C and 5 mbar, had flat surfaces with a rms roughness of about 600 pm. Si was homogeneously incorporated with a flat profile throughout the whole layer at concentration levels ranging from  $5 \times 10^{16} \text{ cm}^{-3}$  to  $3 \times 10^{20} \text{ cm}^{-3}$  proportionally to the used TEOS flux, as evidenced by SIMS measurements. All layers were electrically conductive. However, an unambiguous Hall Effect was measurable only for Si concentrations higher than  $2 \times 10^{18} \text{ cm}^{-3}$ , resulting in electron concentrations from  $1 \times 10^{18} \text{ cm}^{-3}$  to  $2 \times 10^{19} \text{ cm}^{-3}$  at room temperature as shown as red squares in Fig 1. The electron concentration, measurable by the Hall Effect was by a factor of 3 to 30 lower than the dopant concentration measured by SIMS. This indicates a high compensation of the donors by acceptors or a possible incorporation of Si on electrically inactive sites. Compensating acceptors could be point defects (e.g., Ga vacancies) as predicted by literature [3] or extended defects. Above the threshold doping concentration, the mobility decreases from  $30 \text{ cm}^2/\text{Vs}$  to  $10 \text{ cm}^2/\text{Vs}$  for an increase in electron concentration by an order of magnitude, a dependence qualitatively consistent with dominant scattering at ionized impurities. However, these values are reduced by a factor of 5 compared to the electron mobility in conductive bulk samples. For  $n < 1 \times 10^{18} \text{ cm}^{-3}$  the layers are still conductive, but a measurement of the Hall effect is impossible which is ascribed to a sudden drop in electron mobility with decreasing electron concentration (mobility collapse). A similar

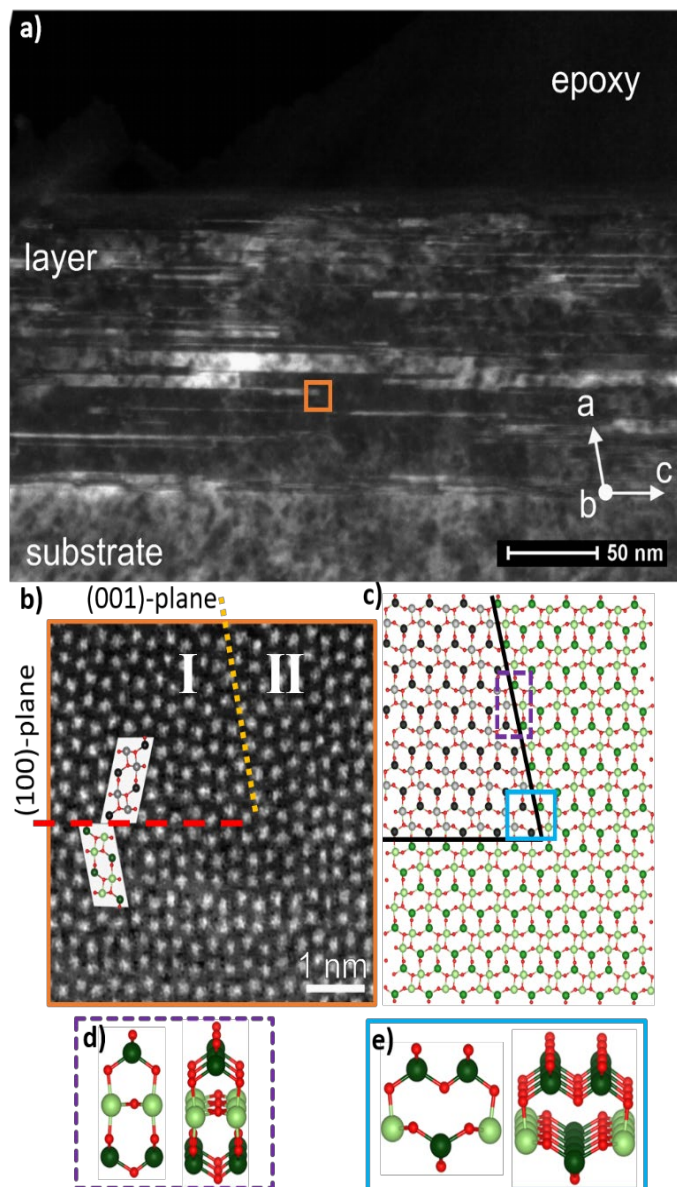


Figure 2 (a) Cross sectional TEM dark field image of a typical MOVPE layer homoepitaxially grown on (100) oriented substrates. For imaging, we used a  $g$  vector parallel to [001]. (b) High resolution STEM-HAADF image showing a region where two twin orientations coalesce. The red dashed line indicates the (100) twin boundary, while the yellow dotted line represents the (001) twin boundary. (c) Structural model of the boundaries developed from the STEM image. Bright green and grey indicating octahedrally bound Ga atoms, and dark green and black correspond to tetrahedrally bound Ga atoms, respectively. Red balls correspond to oxygen atoms. (d) and (e) represent enlarged models of atomic bonding at the (001) boundary corresponding to the, respectively, highlighted structural units in (c). [Image from Fiedler et al. [7]]

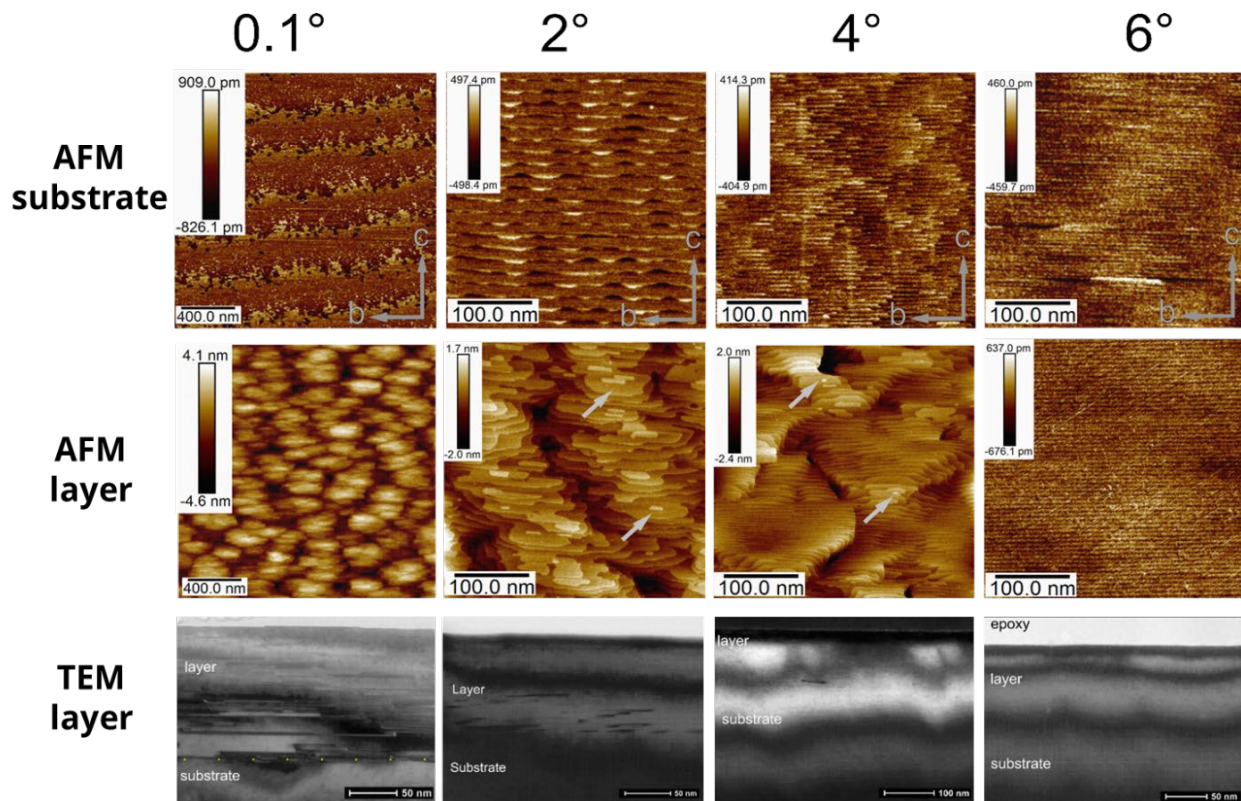


Figure 3 AFM images of substrates with miscut-angles of  $0.1^\circ$ ,  $2^\circ$ ,  $4^\circ$  and  $6^\circ$  towards  $c$  (upper row) and epitaxial grown layers on them (lower row). The substrate is characterized by equally spaced, and regular arranged steps. The surface morphology undergoes a transition from 2D island growth to step-flow growth with increasing miscut-angle. The arrows indicate the presence of two-dimensional islands on the terraces. [image from Schewski et al. [8]]

behavior (reduced mobility and a mobility collapse below a critical carrier concentration) is observed in GaN, where it is explained by the presence of a high density of dislocations forming potential barriers for electron transport. [4,5]

Structural analysis by transmission electron microscopy, as shown in Fig. 2, reveals a high density of twin lamellae in these layers. [6] We observed the same type of defect in MBE grown homoepitaxial  $\text{Ga}_2\text{O}_3(100)$  layers. [13] In contrast to the coherent twin boundaries parallel to the (100) plane, the lateral incoherent twin boundaries exhibit one dangling bond per unit cell that acts as an acceptor-like electron trap. We were able to develop a quantitative model that addresses the influence of incoherent twin boundaries on the electrical properties in  $\beta\text{-Ga}_2\text{O}_3$ . [7] This model can explain the mobility collapse below a threshold electron concentration of  $1 \times 10^{18} \text{ cm}^{-3}$  as well as partly the low doping efficiency in  $\beta\text{-Ga}_2\text{O}_3$  layers grown homoepitaxially by MOVPE on (100) substrates with slight off-orientation. Since the twin lamellae are thin, we consider the incoherent twin boundaries to be line defects with a density of  $10^{11} - 10^{12} \text{ cm}^{-2}$  as determined by TEM. We estimated the influence of the incoherent twin boundaries on the electrical transport properties by adapting Read's model of charged dislocations. As indicated in Fig. 1, our calculations (red shaded area) quantitatively confirm that the mobility reduction and collapse as well as partly the compensation are due to the presence of twin lamellae.

To overcome the deterioration of the electrical properties by the formation of these twin lamellae we studied the dependence of the homoepitaxial growth of  $\beta\text{-Ga}_2\text{O}_3$  on the miscut-angle of the (100) towards the  $c$  direction. [8] Fig. 3 shows atomic force microscopic images of the substrates, the layers as well as TEM bright

field images of these layers. For layers grown on substrates with miscut-angles smaller than 2°, growth proceeds through nucleation and growth of two-dimensional islands. With increasing miscut-angle, step meandering and finally step flow growth takes place. While step-flow growth results in layers with high crystalline perfection, independent nucleation of two-dimensional islands causes double positioning on the (100) plane, resulting in twin lamellae and stacking mismatch boundaries. Applying nucleation theory in the mean field approach for vicinal surfaces, we were able to fit our experimentally found values for the density of twin lamellae in epitaxial layers as a function of miscut-angle. The model yields a diffusion coefficient for Ga adatoms of  $D = 7 \times 10^{-9} \text{ cm}^2 \text{ s}^{-1}$  at a growth temperature of 850°C, which is two orders of magnitude lower than values published for GaAs.[9]

Preventing twin lamella formation requires either the promotion of surface diffusion, which can be achieved by increased growth temperatures or application of surfactants[10], or by the reduction of terrace width by introducing substrates with high miscut-angles. Layers, grown on substrates with appropriate miscut (compare TEM bright field image of layer grown on substrate with 6° miscut in Figure 3), or on substrate orientations that by symmetry do not permit double positioning<sup>11</sup>, do not show twin lamella formation and exhibit an electron mobility similar to the best values observed in bulk crystals (blue dots and triangles in fig. 1).

Summarizing, these investigations led to an improvement of the material quality up to a device grade level, which has enabled the Clusters C3.8 and C3.9 to produce demonstrator devices for the evaluation of  $\beta\text{-Ga}_2\text{O}_3$  for high power electronics

- [1] Z. Galazka, R. Uecker, K. Irmischer, M. Albrecht, D. Klimm, M. Pietsch, M. Brützam, R. Bertram, S. Ganschow, and R. Fornari, *Cryst. Res. Technol.* **45**, 1229 (2010). DOI: [10.1002/crat.201000341](https://doi.org/10.1002/crat.201000341)
- [2] H. Aida, K. Nishiguchi, H. Takeda, N. Aota, K. Sunakawa, and Y. Yaguchi, *Jpn. J. Appl. Phys.* **47**, 8506 (2008). DOI: [10.1143/jjap.47.8506](https://doi.org/10.1143/jjap.47.8506)
- [3] E. Korhonen, F. Tuomisto, D. Gogova, G. Wagner, M. Baldini, Z. Galazka, R. Schewski, and M. Albrecht, *Appl. Phys. Lett.* **106**, 242103 (2015). DOI: [10.1063/1.4922814](https://doi.org/10.1063/1.4922814)
- [4] J.-L. Farvacque, Z. Bougrioua, and I. Moerman, *Phys. Rev. B* **63**, 115202 (2001). DOI: [10.1103/PhysRevB.63.115202](https://doi.org/10.1103/PhysRevB.63.115202)
- [5] S.E. Krasavin, *Semiconductors* **46**, 598 (2012). DOI: [10.1134/S1063782612050132](https://doi.org/10.1134/S1063782612050132)
- [6] G. Wagner, M. Baldini, D. Gogova, M. Schmidbauer, R. Schewski, M. Albrecht, Z. Galazka, D. Klimm, and R. Fornari, *Phys. Status Solidi* **211**, 27 (2014). DOI: [10.1002/pssa.201330092](https://doi.org/10.1002/pssa.201330092)
- \* [7] A. Fiedler, R. Schewski, M. Baldini, Z. Galazka, G. Wagner, M. Albrecht, and K. Irmischer, *J. Appl. Phys.* **122**, 165701 (2017). DOI: [10.1063/1.4993748](https://doi.org/10.1063/1.4993748)
- \* [8] R. Schewski, M. Baldini, K. Irmischer, A. Fiedler, T. Markurt, B. Neuschulz, T. Remmele, T. Schulz, G. Wagner, Z. Galazka, and M. Albrecht, *J. Appl. Phys.* **120**, 225308 (2016). DOI: [10.1063/1.4971957](https://doi.org/10.1063/1.4971957)
- [9] T. Nishinaga and K.I. Cho, *Jpn. J. Appl. Phys.* **27**, L12 (1988). DOI: [10.1143/jjap.27.L12](https://doi.org/10.1143/jjap.27.L12)
- [10] M. Baldini, M. Albrecht, D. Gogova, R. Schewski, and G. Wagner, *Semicond. Sci. Technol.* **30**, 024013 (2015). DOI: [10.1088/0268-1242/30/2/024013](https://doi.org/10.1088/0268-1242/30/2/024013)
- \* [11] M. Baldini, M. Albrecht, A. Fiedler, K. Irmischer, R. Schewski, and G. Wagner, *ECS J. Solid State Sci. Technol.* **6**, Q3040 (2017). DOI: [10.1149/2.0081702jss](https://doi.org/10.1149/2.0081702jss)
- \* [12] N. Ma, N. Tanen, A. Verma, Z. Guo, T. Luo, H. (Grace) Xing, and D. Jena, *Appl. Phys. Lett.* **109**, 212101 (2016). DOI: [10.1063/1.4968550](https://doi.org/10.1063/1.4968550)
- \* [13] Z. Cheng, M. Hanke, Z. Galazka, and A. Trampert, *Nanotechnology* **29**, 395705 (2018). DOI: [10.1088/1361-6528/aad21b](https://doi.org/10.1088/1361-6528/aad21b)

GraFox publications are highlighted by an “\*”.